Monte Carlo analysis of the induced cracked zone by single-hole rock explosion

Mahdi Shadabfar[*1], Hongwei Huang[2a], Yuan Wang[3b] and Chenglong Wu[3c]

[1]Department of Civil Engineering, Sharif University of Technology, Azadi Avenue, Tehran, Iran
[2]Department of Geotechnical Engineering, Tongji University, No. 1239, Siping Road, Shanghai, China
[3]Department of Geotechnical Engineering, Hohai University, No. 1, Xikang Road, Nanjing, China

Abstract. Estimating the damage induced by an explosion around a blast hole has always been a challenging issue in geotechnical engineering. It is difficult to determine an exact dimension for damage zone since many parameters are involved in the formation of failures, and there are some uncertainties lying in these parameters. Thus, the present study adopted a probabilistic approach towards this problem. First, a reliability model of the problem was established and the failure probability of induced damage was calculated. Then, the corresponding exceedance risk curve was developed indicating the relation between the failure probability and the cracked zone radius. The obtained risk curve indicated that the failure probability drops dramatically by increasing the cracked zone radius so that the probability of exceedance for any crack length greater than 4.5 m is less than 5%. Moreover, the effect of each parameter involved in the probability of failure, including blast hole radius, explosive density, detonation velocity, and tensile strength of the rock, was evaluated by using a sensitivity analysis. Finally, the impact of the decoupling ratio on the reduction of failures was investigated and the location of its maximum influence was demonstrated around the blast point.

Keywords: failure probability; cracked zone radius; Monte Carlo method; reliability analysis; exceedance risk curve

1. Introduction

Rock explosions are always associated with a certain extent of damage around the blast hole (Tripathy *et al.* 2016). When the explosive charge is fired, the induced waves rapidly expand through the surrounding environment and severely influence the rock media around the explosion point (Kostic *et al.* 2013). Accordingly, these waves cause the initial borehole to widen and create a set of dense and interconnected cracks around the borehole called the "crushed zone." A few of these cracks penetrate more into the surrounding area and go beyond the crushed zone forming a "cracked zone." Beyond the cracked zone, the impact of explosion is mostly observed as ground vibrations, called the "seismic zone." Thus, the single-hole explosion causes (Esen *et al.* 2003, Lu *et al.* 2016, Liu *et al.* 2017):

• the blast hole to expand,
• the crushed zone to form around the blast hole,
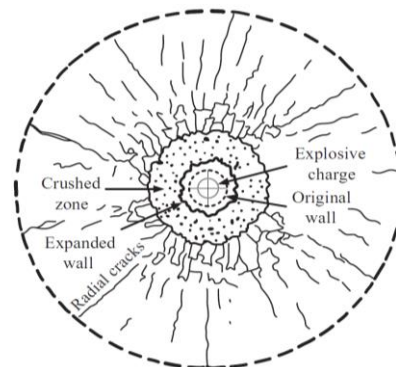• the radial cracks to penetrate through the rock causing

Fig. 1 Crack formation around a blast hole

a cracked zone, and finally,

• the explosion-induced waves to influence the surrounding environment causing some ground vibrations.

Fig. 1 illustrates a schematic plan of the above-mentioned zones around the explosion point.

The induced radial cracks, especially in the perimeter of excavation areas, may impose implementation problems, increase the excavation cost, and raise instability issues (Sun 2013). Thus, optimizing the cracked zone has attracted a lot of attention, and a large body of research has been conducted to estimate the size of the explosion-induced damaged area in rock media (Donze *et al.* 1997, Zhu *et al.* 2007, Sharafisafa *et al.* 2014). Ash (1963, parts 1 and 2) proposed some experimental models to control the undesired outcomes and improve explosion plan. Based on these models, the radius of the damaged area is calculated

---

∗Corresponding author, Ph.D.
  E-mail: mahdishadabfar@yahoo.com
[a]Professor
  E-mail: huanghw@tongji.edu.cn
[b]Professor
  E-mail: wangyuan@hhu.edu.cn
[c]Ph.D.
  E-mail: clongwu88@qq.com

as a coefficient of the blast hole radius by using the relative density of the rock mass and the relative explosive power. In addition, Drukovanyi *et al.* (1973) performed some plane strain analyses for rock mass explosion and determined the distribution of damage zones around the blast hole by using Il'yushin's model for materials and assuming a homogeneous environment. In another study, Xu *et al.* (2004) used several laboratory models to study the effect of radial strains generated in rock-like media and subsequent damage. Further, Hustrulid and Johnson (2008) proposed a model to control the damage caused by both coupled and decoupled explosions. Ma *et al.* (2011) employed a numerical simulation in their study to investigate the pressure load excreted on the blast hole wall. In addition, they studied the damage generated around the explosion point with three different criteria, including Peak Particle Velocity (PPV), Effective Strain (EF), and Damage Criterion. Trivino and Mohanty (2015) implemented a combined FEM-DEM approach to evaluate the damage caused by a single-hole explosion in the rock environment. Then, they presented an experimental model and described the results, compared to the numerical model.

Considering all the above-mentioned studies, the results have more focus on a mean of the measured damage sizes. However, a relatively large difference was observed between the means. In fact, the blasting process has not been recognized well because both rocks and explosives are regarded as complex materials (Nagy *et al.* 2010). Aleatory and/or epistemic uncertainty is applied to both the rock and explosives, leaving the deterministic models unable to provide a unique and comprehensive estimate of failure in rock explosions. Accordingly, a probabilistic approach was adopted in this paper to address the induced damage. In this approach, the involved parameters were first modeled as random variables. This issue reminds us of considering a part of uncertainty associated with the input parameters in our calculations. Then, a reliability analysis was used to calculate the probability of exceedance for cracked zone radius around the blast hole, and to develop the exceedance risk curve. A theoretical foundation for the reliability analysis is explained below.

2. Modeling

In order to perform a reliability analysis, selecting a primary model to estimate the dimension of induced damage seems necessary. In the present study, Senuk's and modified Ash's models were implemented for this purpose (Senuk 1979, Hustrulid 2010). Table 1 indicates the details and proposed relations in these two models, where r_0 represents borehole radius, ρ_0 indicates explosive density, D_{CJ} is regarded as ideal detonation velocity, T presents the tensile strength of the rock material, d_e/d_h shows the ratio of explosive diameter to borehole diameter called "decoupling ratio," *RBS* is the relative bulk strength (compared to ANFO), and ρ_r is described as the density of rock.

Based on the primary models, the rock and explosive characteristics are used as input variables to calculate the size of the cracked zone. However, in order to turn the deterministic model into a probabilistic model and

Table 1 The deterministic models used for approximating the cracked zone radius

Model	Target parameter	Formula
Senuk's Model (Senuk 1979)	Cracked zone radius	$r_c = 1.12 r_0 \sqrt{\rho_0 D_{CJ}^2 /(8T)}$
Modified Ash's Model (Hustrulid 2010)	Cracked zone radius	$r_c = 25 r_0 \dfrac{d_e}{d_h} \sqrt{RBS} \sqrt{2.65/\rho_r}$

Table 2 Characteristics of explosive materials

Sample	Explosive	ρ_0 (g/cm³)	D_{CJ} (m/s)	Source
1	ANFO 1	0.803	5016	Esen *et al.* (2003)
2	WR ANFO	0.994	5829	Esen *et al.* (2003)
3	ANFO 2	0.81	4077	Esen *et al.* (2003)
4	~	1.6	7000	Amnieh and Bahadori (2012b)
5	PETN (10 gr detocord)	1.4	6996	Changshou Sun (2013)
6	ANFO	0.78	4052	Yilmaz and Unlu (2013)
7	Emulsion	1.25	5582	Yilmaz and Unlu (2013)
8	~	1	3600	Lu *et al.* (2014)
9	BA9	1.11	5743	Torbica and Lapčević (2016)
10	BA1_1	1.17	5879	Torbica and Lapčević (2016)
11	BA10_1	0.94	5135	Torbica and Lapčević (2016)
12	BA1_2	1.16	5842	Torbica and Lapčević (2016)
13	BA2_1	1.07	5459	Torbica and Lapčević (2016)
14	Gurit 17	1	~	Iverson et al (2013)
15	Emulit 22	1.13	5000	Iverson et al (2013)
16	ANFO	0.85	~	Iverson et al (2013)
17	Dynamex 32	1.45	4500	Iverson et al (2013)
18	emulsion	1.3	4000	Xie *et al.* (2016)
19	TITAN 2030 (Heavy ANFO)	1.1	~	Blasting Accessories
20	TITAN 3030 (Heavy ANFO)	1.05	~	Blasting Accessories
21	TITAN 4030 (Heavy ANFO)	1.1	~	Blasting Accessories
22	TITAN 5040 (Heavy ANFO)	1.21	~	Blasting Accessories
23	TITAN 5060 (Blend)	1.32	~	Blasting Accessories

Table 3 Means and standard deviations for random variables

Parameter	Mean	Standard deviation
r_0 (mm)	80	30
ρ_0 (gr/cm³)	0.95	0.2
D_{CJ} (m/s)	5000	750
T (Pa)	5,000,000	2,000,000
RBS	1.15	0.1
ρ_r (gr/cm³)	2.5	0.25

formulate the reliability problem, it is necessary to establish

(a) Histogram of explosive density

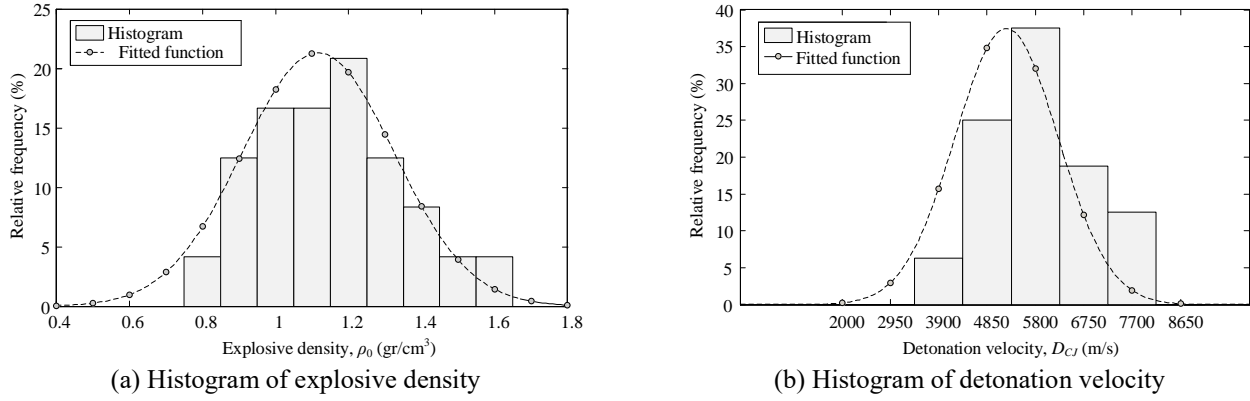(b) Histogram of detonation velocity

Fig. 2 Histograms of (a) explosive density and (b) detonation velocity showing normal distribution of variables

a limit state function (LSF) and define all the involved parameters as random variables with certain means and standard deviations. For this purpose, the LSF was considered as follows:

$$\text{LSF} = R - Q, \qquad (1)$$

where R represents the desired radius of the damage zone (e.g., r_d=2500 mm), and Q is regarded as the estimated length of the radial crack obtained from primary models (r_c). After substituting the two primary models into Eq. (1), two LSFs were defined as follows:

$$\text{LSF}_1 = r_d - 1.12r_0\sqrt{\rho_0 D_{CJ}^2/(8T)}, \qquad (2)$$

$$\text{LSF}_2 = r_d - 25r_0(d_e/d_h)\sqrt{RBS}\sqrt{2.65/\rho_r}. \qquad (3)$$

Now, the probabilistic characteristics of the involved variables should be defined. These characteristics play an important role in uncertainty modeling. In order to match the modeling of random variables with real-world data, 23 caseloads were selected from the literature and the characteristics of the explosive materials, including ρ_0 and D_{CJ}, were listed in Table 2. Then, by providing the histogram for each set of data, it was shown that the normal distribution function could be a proper indicator for the modeling of random variables (Fig. 2). Additionally, referring to the statistical study conducted by Perras and Diederichs (2014) and the histogram provided in their study, it can be found that the tensile strength of rock mass can also be assumed to follow a normal distribution function with a mean close to the one assumed in our paper.

Regarding the other parameters, no direct recommendation is found in the literature about their probabilistic characteristics, and they can take different values depending on the project specification and implementer decision. Therefore, the uniform distribution function that provides a similar probability for different values can be a choice. However, in this paper, a normal distribution was used, with means and standard deviations covering their most common values in real projects. The probabilistic characteristics of all variables are shown in Table 3.

There is still one parameter (d_e/d_h) remaining. This parameter indicates the ratio of the explosive diameter to the borehole diameter called the "decoupling ratio," and this addresses a type of explosion where the explosive charge is not completely fit into the blast hole and a gap is available between them (Zhang 2016). By decreasing the decoupling ratio, an increase takes place in the gap, and a reduction happens in the amount of energy transferred from the explosion to the surrounding rock environment. This issue can significantly decrease the induced damage around the blast hole (Britton 1987, Talhi and Bensaker 2003, Wang 2017). Here, we begin with a full-charge explosion assuming d_e/d_h=1. In Section 4.3, the impact of the decoupling ratio will be discussed in detail.

3. Analysis and results

3.1 Exceedance probability

After establishing LSFs and defining the characteristics of random variables, the Monte Carlo sampling method was employed to calculate the probability of exceedance for cracked zone radius. To do so, by substituting r_d=2500 mm and d_e/d_h=1 in Eqs. (2) and (3), the target LSFs were revised as follows:

$$\text{LSF}_1 = r_d - 1.12r_0\sqrt{\rho_0 D_{CJ}^2/(8T)}, \qquad (4)$$

$$\text{LSF}_2 = r_d - 25r_0(d_e/d_h)\sqrt{RBS}\sqrt{2.65/\rho_r}. \qquad (5)$$

In the next step, 20 random samples were generated by using random characteristics of input variables and their corresponding probability distribution functions. For this purpose, the command normrnd(mu,sigma,m,n) was used in MATLAB programming, where mu represents the mean, sigma indicates the standard deviation, m is regarded as the number of rows, and n shows the number of required columns. For instance, in order to generate 20 random numbers for r_0 with a mean of 80 mm and a standard deviation of 30 mm, we can use this command: r0=normrnd(80,30,20,1). Similarly, this process was repeated for other variables, and 20 random samples were generated for each one. Tables 4 and 5 represent the results of Senuk's and modified Ash's models, respectively. Furthermore, using Eqs. (4) and (5), the LSF values were

Table 4 Generated random samples in Senuk's model

Number	r_0 (mm)	ρ (kg/m³)	D_{CJ} (m/s)	T (Pa)	LSF
1	96.13	1084.30	4923.32	2821871.41	-1173.63
2	135.02	708.50	4818.91	5065114.93	-547.09
3	12.23	1093.45	5239.41	6105054.04	2160.30
4	105.87	1276.05	5234.64	7201220.44	-421.08
5	89.56	1047.78	4351.34	8088423.79	743.58
6	40.77	1156.94	4977.46	5171862.27	1298.16
7	66.99	1095.38	4876.34	2016819.38	-514.67
8	90.28	889.31	5470.78	3515396.33	-610.63
9	187.35	1008.77	5819.95	2876836.53	-5585.18
10	163.08	792.54	5831.95	9700914.45	-904.09
11	39.50	1127.68	4352.26	3768796.24	1322.36
12	171.05	720.59	5058.02	6496153.57	-1108.16
13	101.76	736.23	4089.41	4615162.98	418.71
14	78.11	788.10	4164.87	6777220.85	1110.89
15	101.44	361.14	4994.86	3470301.53	453.22
16	73.85	1237.68	6149.47	2195462.06	-1769.80
17	76.28	1015.04	4422.75	2155248.15	-398.97
18	124.69	799.01	5278.53	5976387.82	-513.55
19	122.27	1224.06	4830.81	4645249.69	-1296.76
20	122.52	607.70	5838.02	4607893.02	-752.54

Table 5 Generated random samples in the modified Ash's model

Number	r_0 (mm)	RBS	ρ_r (gr/cm³)	LSF
1	122.58	1.23	3.23	-584.93
2	88.75	1.06	2.71	238.33
3	85.93	1.16	2.84	266.74
4	127.63	1.10	2.24	-1136.23
5	55.87	1.18	2.38	899.82
6	100.90	1.09	2.43	-249.06
7	105.05	1.20	2.77	-310.47
8	72.69	1.22	2.43	400.78
9	86.47	1.32	2.68	27.03
10	45.02	1.13	1.99	1117.83
11	45.56	0.94	2.41	1344.71
12	83.15	1.07	2.29	193.33
13	101.67	1.29	2.11	-732.76
14	157.56	1.04	2.63	-1540.08
15	59.99	1.25	2.57	800.06
16	85.62	1.16	2.51	127.97
17	77.53	1.29	2.17	62.02
18	22.01	0.95	2.78	1975.49
19	66.83	1.13	2.59	702.45
20	26.16	1.03	2.43	1806.46

calculated for each set of randomly generated numbers. The

Table 6 Exceedance probability for Senuk's and modified Ash's models

Sample number	Senuk's model		Modified Ash's model	
	Less-than-zero number	Exceedance Probability (%)	Less-than-zero number	Exceedance Probability (%)
100	44	44	36	36
500	192	38.4	176	35.2
1000	353	35.3	354	35.4
10000	3671	36.71	3656	36.56
20000	7418	37.09	7238	36.19

results are presented in the last columns of Tables 4 and 5 for Senuk's and modified Ash's models, respectively.

Next, counting the number of less-than-zero samples and dividing it by the total number of samples, the exceedance probability was calculated. As observed in Tables 4 and 5, thirteen and six less-than-zero samples were obtained in each case. Thus, the probability of exceedance for Senuk's (P_1) and modified Ash's (P_2) models is as follows:

$$P_1 = \frac{n}{N} = \frac{13}{20} = 0.65, \tag{6}$$

$$P_2 = \frac{n}{N} = \frac{6}{20} = 0.3. \tag{7}$$

In other words, the probability of exceedance for the cracked zone radius, r_c=2500 mm, was calculated as 65% and 30% for Senuk's and modified Ash's models, respectively. However, these values cannot yet be accepted as the final output because the number of random samples used in their calculation is limited, and the results may depend on the number of samples. In order to solve this problem, it is required to increase the number of samples to ensure that more increases in the sample number cannot change the results. Thus, the above calculations were repeated for the sample numbers 100, 500, 1000, 10,000, and 20,000. Table 6 indicates the results for both Senuk's and modified Ash's models.

In order to clearly observe the convergence process and ensure the accuracy of the output, by taking a relatively smaller step than that in Table 6, the above calculations were repeated and the number of samples was drawn against the exceedance probability. What is meant by the step in this section is the difference between each two decision variables reported in the first column of Table 6. Figs. 3(a) and 3(b) illustrate the results for Senuk's and modified Ash's models, respectively. A y-axis limit was applied to this figure to provide a clearer view of the graph.

As observed, by increasing the number of samples to 20,000, the probabilities for Senuk's and modified Ash's models are converged to 37.09% and 36.19%, respectively. Having these results, the primary goal of the study to calculate the exceedance probability of the cracked zone was achieved. However, this only shows the probability of exceedance for R=2500 mm. For a more comprehensive
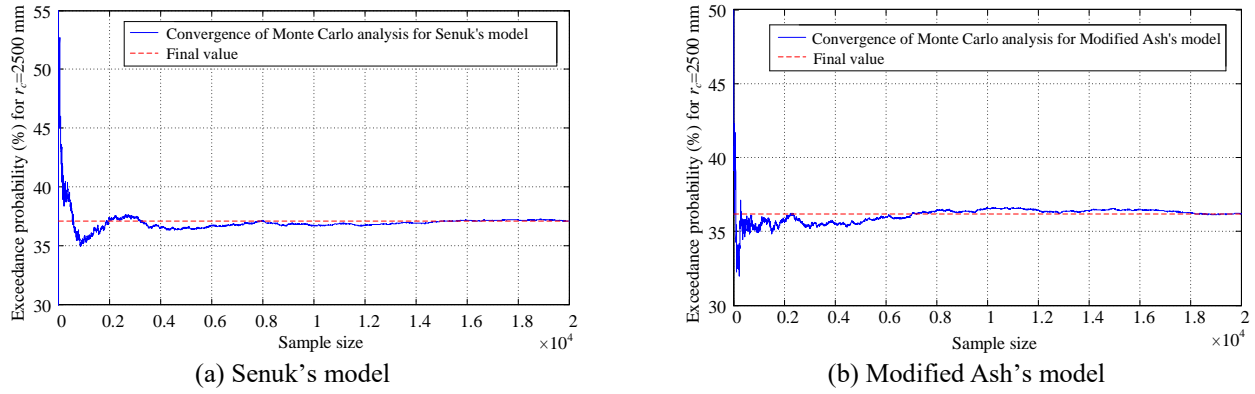
(a) Senuk's model　　　　　　　　　　　　(b) Modified Ash's model

Fig. 3 Convergence of the Monte Carlo analysis
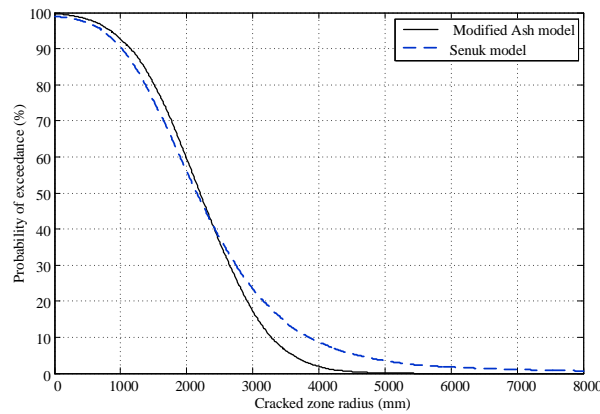
Fig. 4 Exceedance risk curve for both Senuk's and modified Ash's model

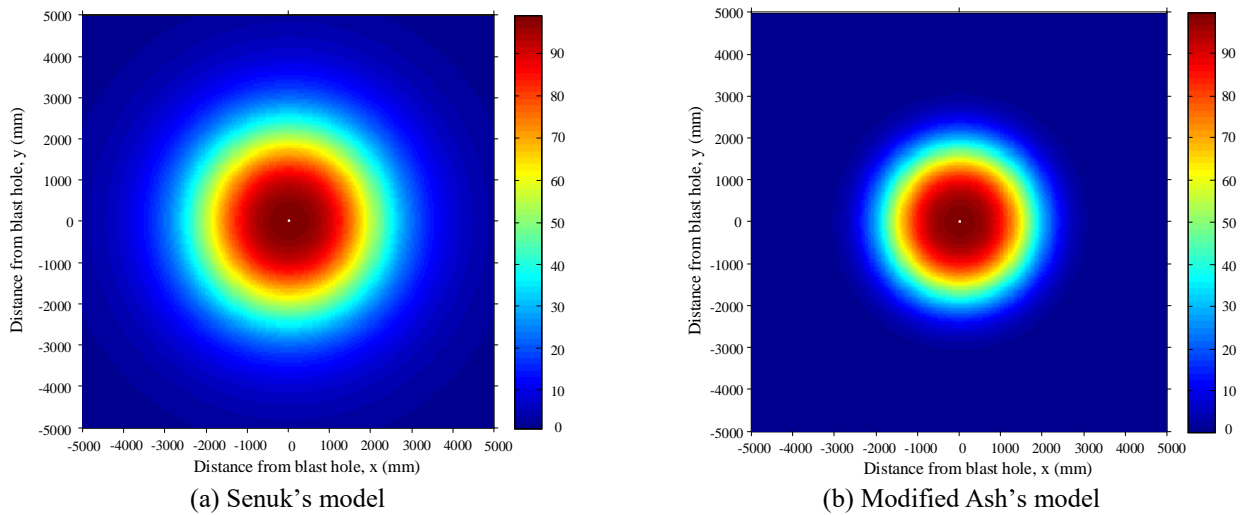(a) Senuk's model　　　　　　　　　　　　(b) Modified Ash's model

Fig. 5 Contour plot for the exceedance probability of cracked zone radius around the explosion point

assessment of the failure probability around the blast hole, the probability of exceedance for any desired distance from the blast hole should be targeted. In other words, each desired cracked zone radius should be related to an exceedance probability.

3.2 Exceedance risk curve

In the previous section, the reliability problem for R=2500 mm was solved and the corresponding probability was calculated. Now, the probability of exceedance should be calculated for any desired radius. Hence, R is considered as the decision variable, r_d. By changing the r_d, the LSF is updated, and a new reliability problem is established which needs to be analyzed separately. Using 20,000 random samples, this process was performed for several different values of r_d. Table 7 represents the results for both Senuk's and modified Ash's models.

Based on this approach, each value of the decision variable, r_d, corresponds to a probability of exceedance.

Table 7 Exceedance probability for different values of r_d

Decision variable	Senuk's model		Modified Ash's model	
	Less-than-zero number	Exceedance Probability (%)	Less-than-zero number	Exceedance Probability (%)
100	19797	98.98	19888	99.44
500	19455	97.27	19612	98.06
1000	18170	90.85	18547	92.73
1500	15094	75.47	15966	79.83
2000	11059	55.29	11895	59.47
2500	7409	37.04	7177	35.88
3000	4575	22.87	3410	17.05
3500	2785	13.92	1306	6.53
4000	1689	8.44	380	1.90
8000	127	0.63	0	0

Choosing a step smaller than that in Table 7 (i.e., the difference between each two decision variables listed in the first column), r_d was depicted against P_f and a graph was fitted to them. Fig. 4 illustrates the graph for both Senuk's and modified Ash's models, known as the "exceedance risk curve" (Nikolaidis *et al.* 2005).

As observed in Fig. 4, the probability of exceedance drops sharply by increasing the damage zone radius. For instance, in the graph related to modified Ash's model, the failure probability of 50% for r_c=2.20 m drops to 10% for r_c=3.28 m and further to 1% for r_c=4.21 m. The probability of exceedance for r_c=3.62 m in modified Ash's model and r_c=4.56 m for the Senuk's model is less than 5% (These values are directly resulted from analysis; but, can roughly be read from Fig. 4 as well). This shows that cracked zone radii larger than 4.5 m are unlikely to occur. As shown in Fig. 4, the modified Ash's model gives a higher result than Senuk's model for cracked zone radii less than 2.44 m, while less chance is estimated for cracks to propagate inside the rock for radii larger than 2.44 m. In other words, a higher risk curve results in increasing the chance of damage to grow inside the rock mass. Therefore, the modified Ash's model provides a more optimistic estimate of rock capacity to accommodate the explosion load for large damage zone radii (larger than 2.44 m), compared to those of Senuk's model. Optimistic estimate means that the modified Ash's model reports a lower probability of exceedance for a given length of radial cracks than Senuk's model. In fact, the cracked zone has less chance to grow through the rock under the explosion load, indicating a higher load-bearing capacity of rock mass to withstand the explosion load. However, the amount of difference is gradually decreasing, and accordingly the two graphs become tangent for very large radii.

3.3 Contour plot of exceedance risk curve

The risk curves shown in Fig. 4 provided useful information about the probability of failure due to the explosion. However, a physical aspect of the problem cannot be easily understood from this figure. Therefore,

instead of using the graph form, these two graphs were represented as contour plots around the explosion point. Figs. 5(a) and 5(b) illustrate the contour of exceedance probability obtained from Senuk's and modified Ash's model, respectively. As displayed, by getting farther from the explosion point, the exceedance probability decreases sharply. This occurs more quickly in the modified Ash's model, compared to Senuk's model. In fact, Fig. 5(b) illustrates a comparatively smaller area indicating less chance for the cracked zone to infiltrate the rock. This proves the point that modified Ash's model provides a more optimistic estimate of rock capacity against failure, compared to Senuk's model.

4. Discussion

4.1 Accuracy of Monte Carlo method

As already mentioned, the accuracy of the Monte Carlo method relies heavily on the sample size used in the calculations. In fact, an increase in the number of random samples leads to an increase in the accuracy of the Monte Carlo method and consequently causes the failure probability to converge to a specific answer (Nowak and Collins 2013, Cardoso *et al.* 2008). This matter could be examined using the exceedance risk curve. For such purpose, the Monte Carlo method was adopted by using 20, 50, 100, 500, 1000, and 20,000 random samples to calculate the exceedance risk curve by Senuk's model. The results are shown in Fig. 6.

As observed, the graph is similar to a "floor and ceiling function" for low sample numbers, indicating a high variance in outputs so that the analysis could not obtain an accurate result. Then, the graph got smoother when the sample size increased to 100 and then 500, although a fluctuation was still observed. In the next stage, when the sample number increased to 1000 and then 20,000, a smooth and continuous graph was obtained, which could approximate with acceptable accuracy the failure probability for any desired radius.

4.2 Sensitivity analysis

The effect of each parameter involved in generating failures around the blast hole is regarded as one of the important issues which should be emphasized.

This issue, however, may not be easily measured by deterministic methods. Reliability analysis is regarded as a more powerful tool for this purpose. Therefore, Senuk's model was implemented and accordingly a reliability sensitivity analysis was conducted. To this end, by changing the mean of one parameter and keeping the others constant, the reliability analysis was repeated and the exceedance probability was displayed against the cracked zone radius. Thus, a risk curve was obtained for each of the assumed mean of the target parameter. Figs. 7(a)-7(d) illustrate the related diagrams for the involved parameters, including blast hole radius, r_0, explosive density, ρ_0, ideal detonation velocity, D_{CJ}, and tensile strength of the rock, T, respectively.
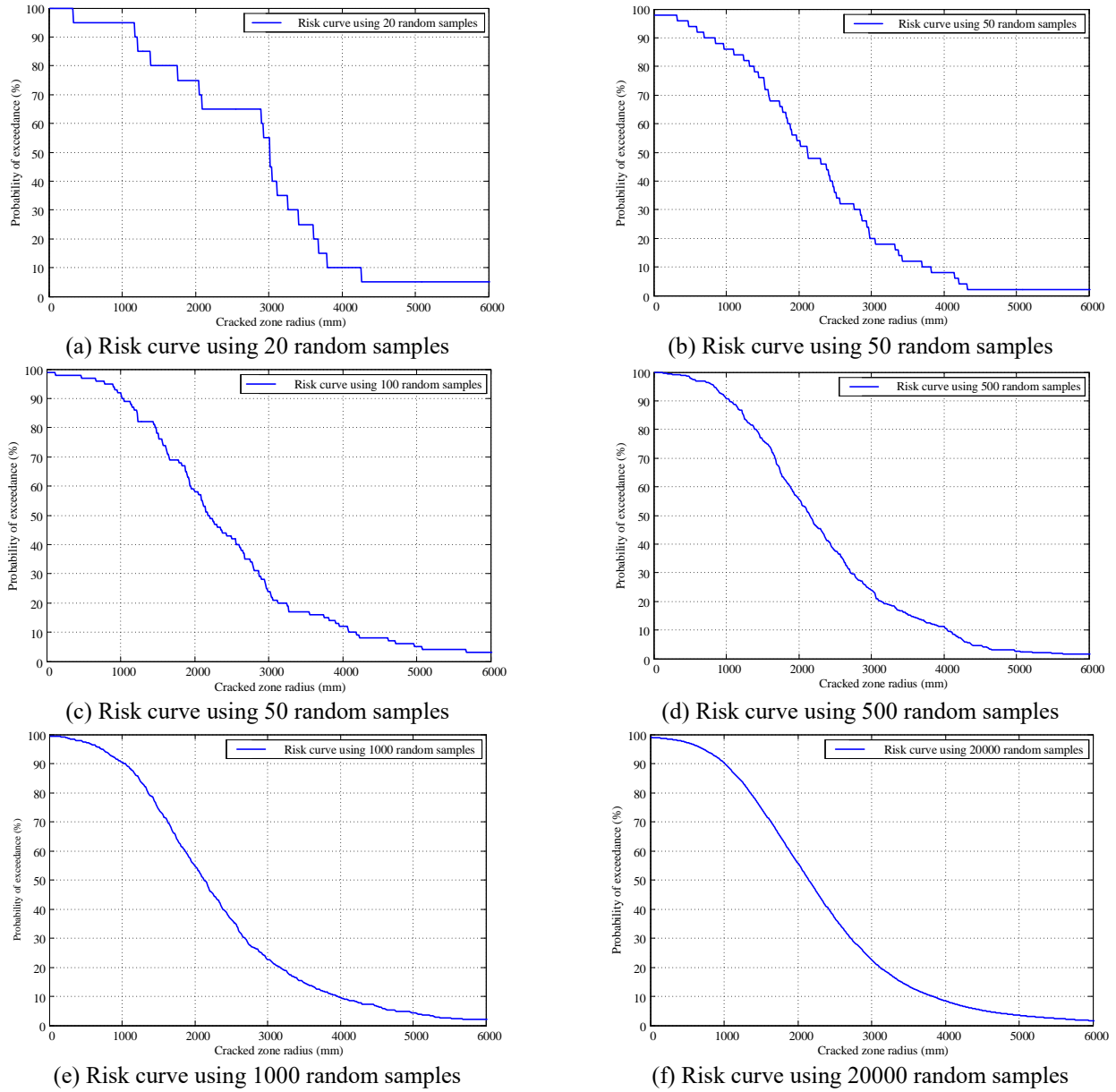
As seen, the change of parameters influences the entire

(a) Risk curve using 20 random samples

(b) Risk curve using 50 random samples

(c) Risk curve using 50 random samples

(d) Risk curve using 500 random samples

(e) Risk curve using 1000 random samples

(f) Risk curve using 20000 random samples

Fig. 6 Effect of sample size on exceedance risk curve

(a) Risk curves for different blast hole radii

(b) Risk curves for different explosive densities
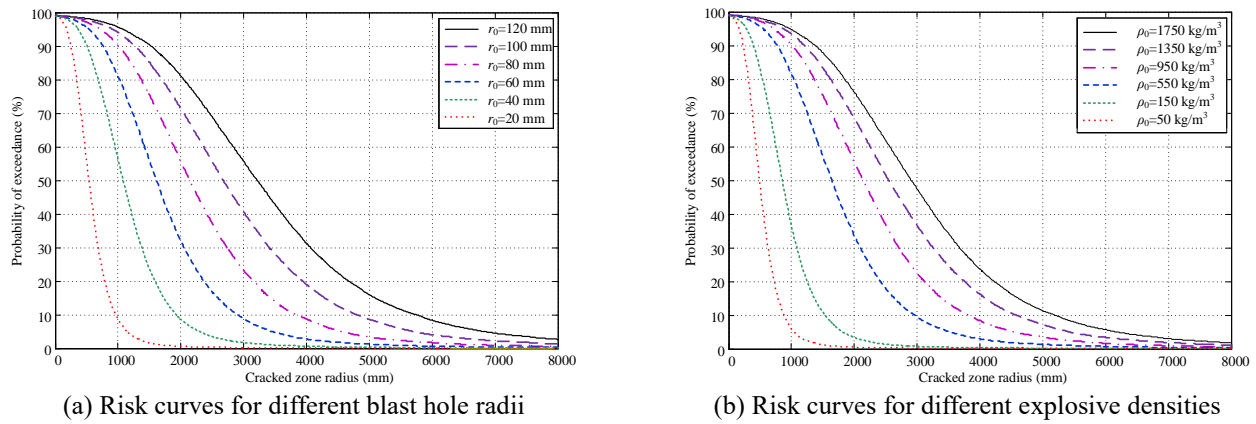
Fig. 7 Effect of different parameters: (a) blast hole radius, (b) explosive density, (c) detonation velocity, and (d) tensile strength of the rock on exceedance risk curve
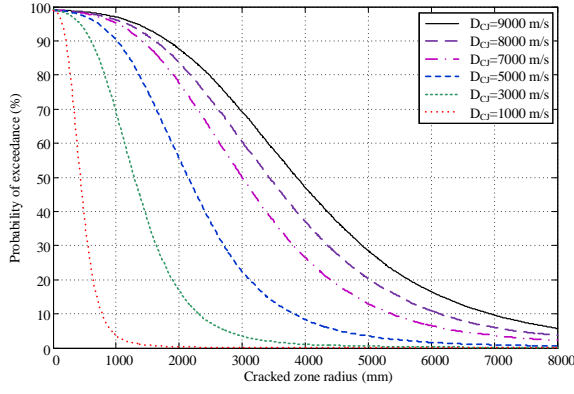
(c) Risk curves for different detonation velocities
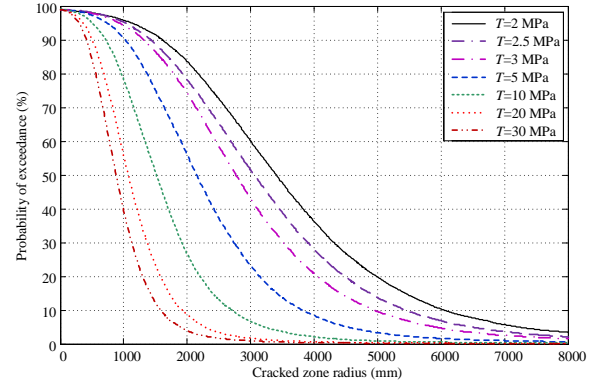
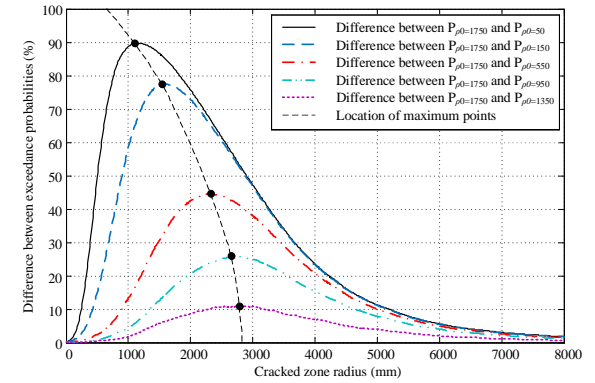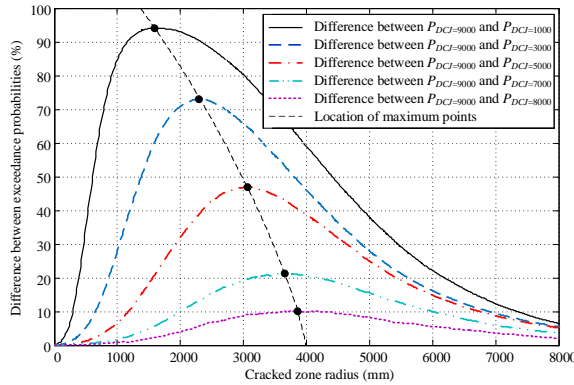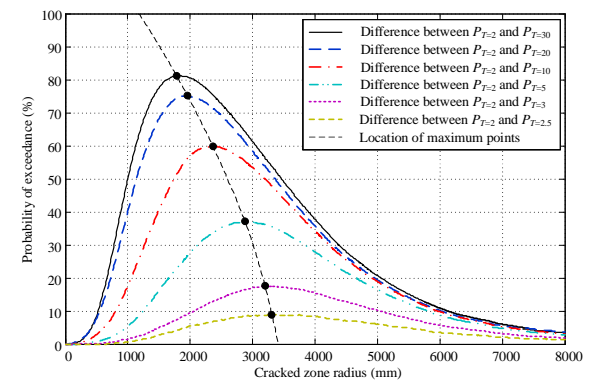(d) Risk curves for different tensile strengths

Fig. 7 Continued
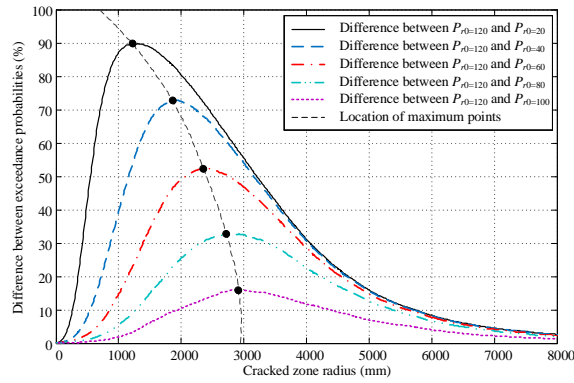
(a) Difference between probabilities with respect to r_0

(b) Difference between probabilities with respect to ρ_0

(c) Difference between probabilities with respect to D_{CJ}

(d) Difference between probabilities with respect to T

Fig. 8 Difference between exceedance probabilities with respect to (a) blast hole radius, (b) explosive density, (c) detonation velocity, and (d) tensile strength of the rock

range of the damage zone. An increase in r_0, ρ_0, and D_{CJ} results in enhancing the probability of failure while an increase in T leads to a decrease in the failure probability. Now, in order to further study the impact of different parameters, the difference between the risk curves corresponding to different mean values were calculated and plotted on a new graph separately. As the first parameter, we considered the blast hole radius, r_0. The difference between the exceedance probability corresponding to r_0=120 mm and other cases were calculated as follows:

$$\Delta P = P_{r=120} - P_r, \qquad (8)$$

where ΔP represents the difference between the exceedance

probabilities, P_r indicates the probability corresponding to r_0=20, 40, 60, 80, or 100 mm, and $P_{r=120}$ is regarded as the probability related to r_0=120 mm. Using this formula, the difference between exceedance risk curves was plotted in Fig. 8(a). As observed, the maxima of graphs take place in a short range of cracked zone radii, roughly between 700 and 2950 mm, indicating that the change in the blast hole radius affects mostly cracked zones with small size, being less effective for large-size cracked zones. Adopting a similar method, the change in exceedance probabilities for different explosive densities, ρ_0, was evaluated as follows:

$$\Delta P = P_{\rho_0=1750} - P_{\rho_0}, \qquad (9)$$

(a) Effects of blast hole radius

(b) Effects of explosive density

(c) Effects of detonation velocity
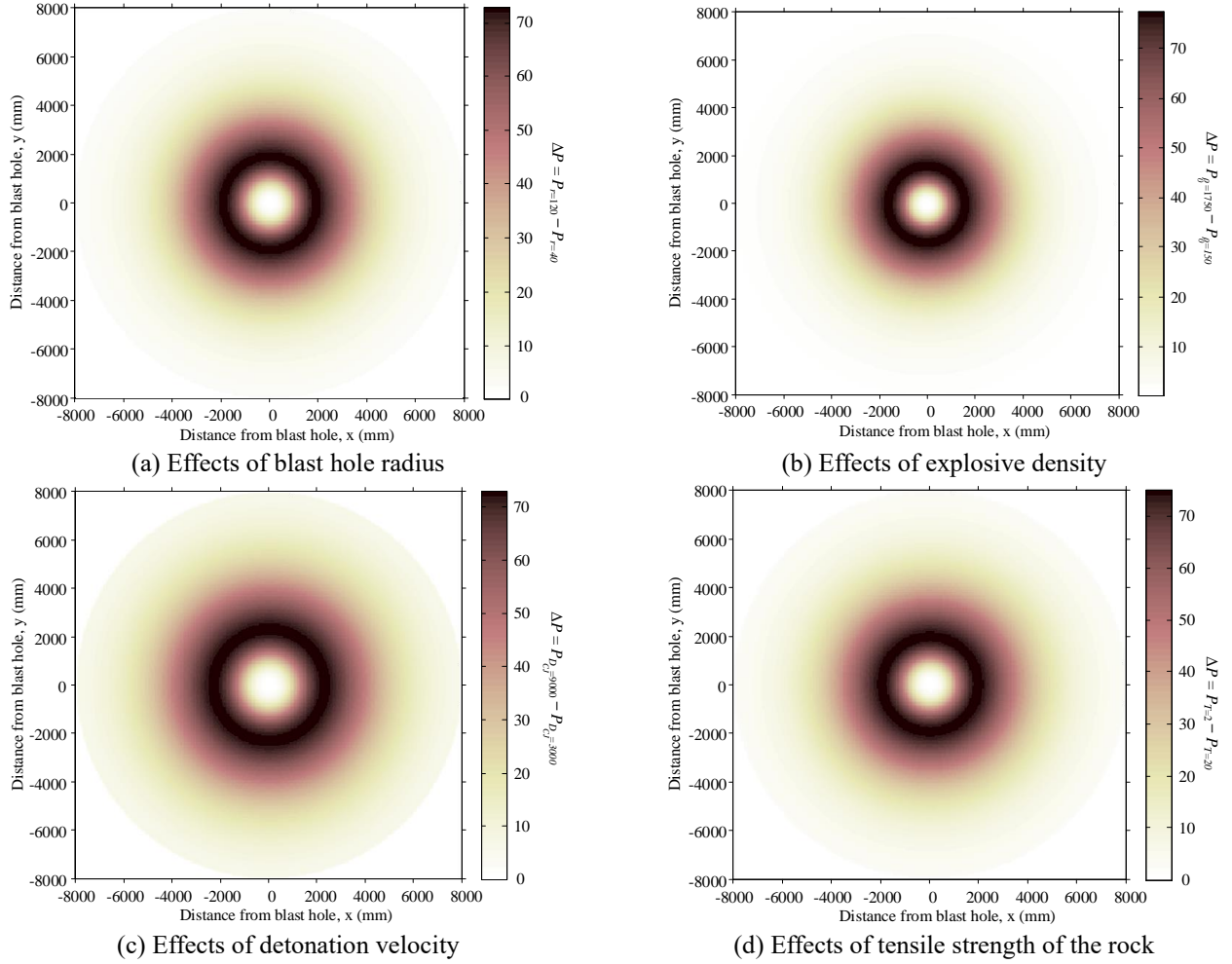

(d) Effects of tensile strength of the rock

Fig. 9 Location of the maximum influences of (a) blast hole radius, (b) explosive density, (c) detonation velocity, and (d) tensile strength of the rock around the explosion point

where ΔP indicates the difference between exceedance probabilities, $P_{\rho 0}$ represents the probability corresponding to $\rho_0 = 50$, 150, 550, 950 or 1350 kg/m^3, and $P_{\rho 0}$=1750 is considered as the probability corresponding to ρ_0=1750 kg/m^3. Fig. 8(b) depicts the difference between exceedance risk curves. Based on the results, similar to the previous case, it was found that explosive density could influence a short range of radii, between 700 to 2900 mm. The impact of ρ_0 decreases significantly for very small or very large radii. In a similar way, ΔP for different detonation velocities, D_{CJ}, was calculated using Eq. (10):

$$\Delta P = P_{D_{CJ}=9000} - P_{D_{CJ}}, \qquad (10)$$

where $P_{D_{CJ}}$=9000 indicates the probability corresponding to D_{CJ}=9000 m/s, and $P_{D_{CJ}}$ represents the probability corresponding to D_{CJ}=1000, 3000, 5000, or 7000 m/s. Fig. 8(c) illustrates the difference between exceedance risk curves. As shown, a long range of cracked zones radii, roughly between 1400 to 4000 mm, was influenced more by detonation velocity. Finally, Eq. (11) was used to repeat the same process for the tensile strength of the rock, T.

$$\Delta P = P_{T=2} - P_T, \qquad (11)$$

where P_T=2 represents the probability corresponding to T=2 MPa, and P_T indicates the probability of T=2.5, 3, 5, 10, 20 or 30 MPa. Fig. 8(d) illustrates the difference between exceedance risk curves. Based on the results, the tensile strength of the rock approximately affects an average range of cracked zone radii, ranging from 1200 to 3400 mm.

Instead of using graphs to show the difference between the risk curves, contour plots were drawn for illustrating the location of maximum influence of each parameter around the explosion point. Fig. 9 illustrates the plots for all four parameters involved.

It seems that the maximum effect of each parameter falls within a particular range of the damaged zone radius. The blast hole radius and explosive density highly influence the small cracked zone radii, while the maximum effect of detonation velocity is in the medium range of cracked zone radii. Further, the tensile strength of the rock has a greater effect on the longer cracked zone radii. In fact, based on the data analysis, the explosion characteristics (r_0, ρ_0, and D_{CJ}) play a significant role on the small and medium range radii and are less influential in large radii. However, the rock characteristics (T) fail to represent significant resistance against explosion in areas close to the blast hole, being more effective for large cracked zone radii.

(a) Risk curves for different d_e/d_h

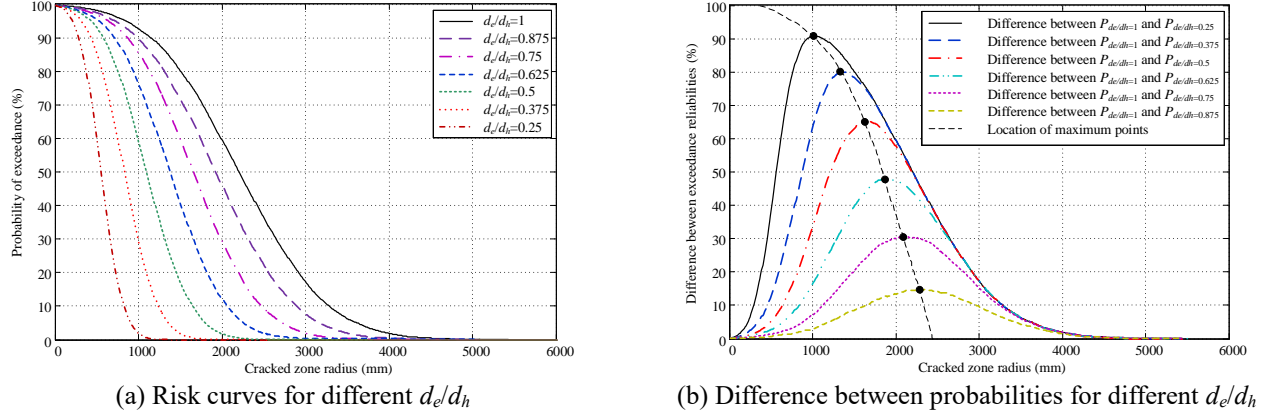(b) Difference between probabilities for different d_e/d_h

Fig. 10 Effect of the decoupling ratio on failure probability

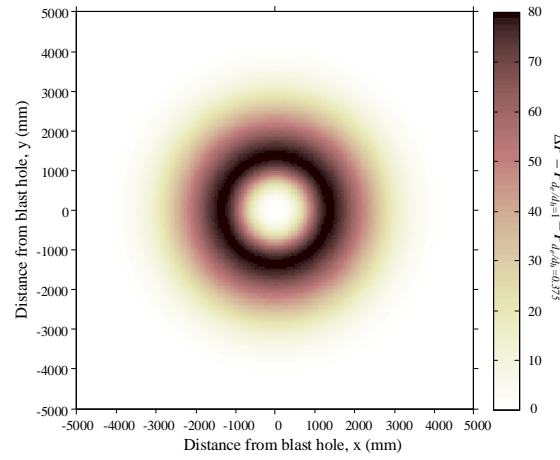Fig. 11 Location of maximum influence of decoupling ratio around the explosion point

4.3 Effect of decoupling on the size of cracked zone

As it was already mentioned, a gap is created between the explosive and borehole wall if the explosion charge has a smaller radius than the blast hole. The gap can effectively dissipate the energy released from the explosion and consequently reduce the effect of the explosion in the surrounding environment. This topic has been investigated by various researchers referred to as "decoupled explosion." For instance, based on measurements made in the Aspo excavation area, where different decoupling ratios were used on the roofs and walls, the dimensions of the cracks formed around the explosion points were relatively different (Emsley *et al.* 1997).

The results indicated that the decoupling ratio is directly proportional to the dimension of the induced damage as follows (Zhang 2016):

$$r_c = k \times \frac{d_e}{d_h}, \qquad (12)$$

where r_c represents the cracked zone radius, d_e/d_h indicates the decoupling ratio, and k is regarded as a constant parameter. Although the result of such empirical measurements may be useful for estimating the dimension of the failure, it fails to provide a comprehensive understanding of the decoupling effect and the interaction

between the explosion wave and the borehole wall. Thus, similar to the process described in the previous section, a sensitivity reliability analysis was performed on the modified Ash's model in order to examine how the decoupling ratio can influence the failure probability. For this purpose, by assuming seven different values of decoupling ratio and considering the other parameters as constant, the exceedance probability was drawn against the cracked zone radius. Fig. 10(a) illustrates the graph for various values of d_e/d_h.

As observed, a decrease in d_e/d_h drastically reduces the probability of failure. This complies with the results of some deterministic studies available in the literature (Britton 1987, Nie 1999, Liang *et al.* 2012). Then, the range of the cracked zone radius where the impact of the decoupling ratio was maximum was studied by calculating the difference between risk curves. Fig. 10(b) illustrates the results of the difference between the exceedance probabilities against the cracked zone radius.

In the next step, the figure was changed into the equivalent contour plot, as shown in Fig. 11. Clearly, the decoupling ratio imposes maximum effects on radial cracks of 400-2400 mm in length. Beyond this range, the impact of the decoupling ratio is insignificant.

It should be noted that the reliability sensitivity analysis (Section 4.2) is reported only for Senuk's model. The reason for this matter is that the variables involved in

Senuk's model (i.e., r_0, ρ_0, D_{CJ}, and T) are among the most important and well-known parameters in geotechnical projects. Therefore, their influence on failure probability seems to be interesting for readers. However, the variables involved in modified Ash's model, such as RBS, are not commonly used by engineers. Therefore, this section is only devoted to Senuk's model. Of course, following the steps provided in the paper, similar analyses can be conducted for Modified Ash's model. The decoupling effects (Section 4.3), however, are only presented for Modified Ash's model. The reason for this point is that the decoupling ratio is only available in Modified Ash's model. In fact, Senuk's model does not consider this parameter and, therefore, is unable to assess its effects.

5. Conclusions

In the present study, the Monte Carlo method was employed to investigate the induced cracked zone around a blast hole in rock. For this purpose, LSF functions were first established based on Senuk's and modified Ash's models, and then the problem was analyzed using the reliability method. Subsequently, the results were plotted in the form of a failure probability against the cracked zone radius. The obtained graph, the "exceedance risk curve," represented a probability of failure for any desired length of radial cracks.

Based on the results, the following conclusions were drawn:

• The modified Ash's model reported a larger failure probability than Senuk's model for damage zone radii shorter than 1.44 m. For larger radii, the result was reversed and the modified Ash's model yielded smaller results. Furthermore, the difference reduced gradually so that the risk curves obtained from the two models became tangent for very large cracked zone radii.

• Based on the presented risk diagrams, the probability of failure dropped sharply by increasing the cracked zone radius so that the probability corresponding to cracked zone radii larger than 4.5 m was less than 5%, and thus very unlikely to happen.

• The greatest impact of the explosion characteristics, including the blast hole radius, explosive density, and detonation velocity, fell within the range of small to medium damaged zone radii between 700 to 3400 mm, while the parameters corresponding to the rock characteristics, such as tensile strength of the rock mass, mostly affected large radii within the range of 1400 to 4000 mm.

• The size of the explosion induced damage was sharply reduced by increasing the distance between the explosive charge and the borehole wall. Further, the greatest impact of the decoupling ratio occurred within the range of 400 to 2400 mm while an insignificant effect was represented beyond this range.

Last but not least, the involved parameters were assumed independent in the present study. Therefore, further research can be conducted to study the correlation between the parameters by considering the correlation matrix into calculation. This topic will be studied by the authors in their future research.

References

Ash, R.L. (1963), "The mechanics of rock breakage (part 2), standards for blasting design", *Pit Quarry*, **56**(3), 118-122.

Ash, R.L. (1963), "The mechanics of the rock breakage (part 1)", *Pit Quarry*, **56**(2), 98-100.

BakhshandehAmnieh, H. and Bahadori, M. (2012), "Numerical and field analysis of single-hole blasting mechanism in conglomerate rock mass of Gotvand Olya Dam", *Energy Eng. Manage.*, **2**(1), 22-31.

Blasting Accessories (2010), Blasting and Explosives Quick Reference Guide, Dyno Nobel. https://www.yumpu.com/en/document/view/4652050/blasting-and-explosives-quick-reference-guide-2010-dyno-nobel.

Britton, R.R. (1987), "Effect of decoupling ratio on explosive-generated energy release", Ph.D. Dissertation, The Ohio State University, Columbus, Ohio, U.S.A.

Cardoso, J.B., de Almeida, J.R., Dias, J.M. and Coelho, P.G. (2008), "Structural reliability analysis using Monte Carlo simulation and neural networks", *Adv. Eng. Softw.*, **39**(6), 505-513. https://doi.org/10.1016/j.advengsoft.2007.03.015.

Donze, F.V., Bouchez, J. and Magnier, S.A. (1997), "Modeling fractures in rock blasting", *Int. J. Rock Mech. Min. Sci.*, **34**(8), 1153-1163. https://doi.org/10.1016/S1365-1609(97)80068-8.

Drukovanyi, M.F., Komir, V.M., Myachina, N.I., Rodak, S.N. and Semenyuk, E.A. (1973), "Effect of the charge diameter and type of explosive on the size of the overcrushing zone during an explosion", *J. Min. Sci.*, **9**(5), 500-506. https://doi.org/10.1007/BF02501378.

Emsley, S., Olsson, O., Stenberg, L., Alheid, H.J. and Falls, S. (1997), "ZEDEX - A study of damage and disturbance from tunnel excavation by blasting and tunnel boring", No. SKB-TR--97-30, Swedish Nuclear Fuel and Waste Management Co., Stockholm, Sweden.

Esen, S., Onederra, I. and Bilgin, H.A. (2003), "Modelling the size of the crushed zone around a blast hole", *Int. J. Rock Mech. Min. Sci.*, **40**(4), 485-495. https://doi.org/10.1016/S1365-1609(03)00018-2.

Hu, Y., Lu, W., Chen, M., Yan, P. and Yang, J. (2013), "Comparison of blast-induced damage between presplit and smooth blasting of high rock slope", *Rock Mech. Rock Eng.*, **47**(4), 1307-1320. https://doi.org/10.1007/s00603-013-0475-7.

Hustrulid, W. (2010), "Some comments regarding development drifting practices with special emphasis on caving applications", *Min. Technol.*, **119**(3), 113-131. https://doi.org/10.1179/174328610X12820409992219.

Hustrulid, W. and Johnson, J. (2008), "A gas pressure-based drift round blast design methodology", *Proceedings of the 5th International Conference and Exhibition on Mass Mining*, Lulea, Sweden, June.

Iverson, S.R., Hustrulid, W.A. and Johnson, J.C. (2013), "A new perimeter control blast design concept for underground metal/nonmetal drifting applications", Technical Report, National Institute for Occupational Safety and Health, Office of Mine Safety and Health Research.

Kostić, S., Perc, M., Vasović, N. and Trajković, S. (2013), "Predictions of experimentally observed stochastic ground vibrations induced by blasting", *PLoS ONE*, **8**(12), 1-13. https://dx.doi.org/10.1371%2Fjournal.pone.0082056b.

Liang, W.M., Liu, H.Y. and Zhou, F.J. (2012), "Influence of air-decoupling charge on rock blasting", *Trans. Beijing Inst. Technol.*, **32**(12), 1215-1218.

Liu, C.Y., Yang, J.X. and Yu, B. (2017), "Rock-breaking mechanism and experimental analysis of confined blasting of borehole surrounding rock", *Int. J. Min. Sci. Technol.*, **27**(5), 795-801. https://doi.org/10.1016/j.ijmst.2017.07.016.

Lu, W., Leng, Z., Chen, M., Yan, P. and Hu, Y. (2016), "A

modified model to calculate the size of the crushed zone around a blast-hole", *J. South. Afr. Inst. Min. Metall.*, **116**(5), 413-422. http://dx.doi.org/10.17159/2411-9717/2016/v116n5a7.

Ma, G.W., Hao, H. and Wang, F. (2011), "Simulations of explosion-induced damage to underground rock chambers", *J. Rock Mech. Geotech. Eng.*, **3**(1), 19-29. https://doi.org/10.3724/SP.J.1235.2011.00019.

Nagy, N., Mohamed, M. and Boot, J.C. (2010), "Nonlinear numerical modelling for the effects of surface explosions on buried reinforced concrete structures", *Geomech. Eng.*, **2**(1), 1-18. http://doi.org/10.12989/gae.2010.2.1.001.

Nie, S. (1999), "Measurement of borehole pressure history in blast holes in rock blocks", *Fragblast 1999*.

Nikolaidis, E., Ghiocel, D.M. and Singhal, S. (2005), *Engineering Design Reliability*, CRC Press, Taylor and Francis.

Nowak, A.S. and Collins, K.R. (2013), *Reliability of Structures*, CRC Press, Taylor and Francis.

Perras, M.A. and Diederichs, M.S. (2014), "Predicting excavation damage zone depths in brittle rocks", *J. Rock Mech. Geotech. Eng.*, **8**(1), 60-74. https://doi.org/10.1016/j.jrmge.2015.11.004.

Senuk, V.M. (1979), "The impulse from an explosion, and conditions for its greater utilization in crushing hard rock masses in blasting", *Soviet Min. Sci.*, **15**(1), 22-27. https://doi.org/10.1007/BF02499637.

Sharafisafa, M., Aliabadian, Z., Alizadeh, R. and Mortazavi, A. (2014), "Distinct element modelling of fracture plan control in continuum and jointed rock mass in presplitting method of surface mining", *Int. J. Min. Sci. Technol.*, **24**(6), 871-881. https://doi.org/10.1016/j.ijmst.2014.10.022.

Sun, C. (2013), "Damage zone prediction for rock blasting", Ph.D. Dissertation, The University of Utah, Salt Lake City, Utah, U.S.A.

Talhi, K. and Bensaker, B. (2003), "Design of a model blasting system to measure peak p-wave stress", *Soil Dyn. Earthq. Eng.*, **23**(6), 513-519. https://doi.org/10.1016/S0267-7261(03)00018-6.

Torbica, S. and Lapčević, V. (2016), "Fragmenting of cylindrical rock specimens under explosive load: Comparison between model and laboratory results", *Min. Metall. Inst. Bor*, **1**, 103-114.

Tripathy, G.R., Shirke, R.R. and Kudale, M.D. (2016), "Safety of engineered structures against blast vibrations: A case study", *J. Rock Mech. Geotech. Eng.*, **8**(2), 248-255. https://doi.org/10.1016/j.jrmge.2015.10.007.

Trivino, L.F. and Mohanty, B. (2015), "Assessment of crack initiation and propagation in rock from explosion-induced stress waves and gas expansion by cross-hole seismometry and FEMDEM method", *Int. J. Rock Mech. Min. Sci.*, **77**, 287-299. https://doi.org/10.1016/j.ijrmms.2015.03.036.

Wang, Y. (2017), "Study of the dynamic fracture effect using slotted cartridge decoupling charge blasting", *Int. J. Rock Mech. Min. Sci.*, **96**, 34-46. https://doi.org/10.1016/j.ijrmms.2017.04.015.

Xie, L.X., Lu, W.B., Zhang, Q.B., Jiang, Q.H., Wang, G.H. and Zhao, J. (2016), "Damage evolution mechanisms of rock in deep tunnels induced by cut blasting", *Tunn. Undergr. Sp. Technol.*, **58**, 257-270. https://doi.org/10.1016/j.tust.2016.06.004.

Xu, G.Y., Duan, L.Z., Gu, D.S. and Yan, C.B. (2004), "Radial explosion strain and its fracture effect from confined explosion with charge of cyclonite", *J. Central South Univ. Technol.*, **11**(4), 429-433. https://doi.org/10.1007/s11771-004-0089-z.

Yilmaz, O. and Unlu, T. (2013), "Three dimensional numerical rock damage analysis under blasting load", *Tunn. Undergr. Sp. Technol.*, **38**, 266-278. https://doi.org/10.1016/j.tust.2013.07.007.

Zhang, Z.X. (2016), *Chapter 10 – Single-Hole Blasting*, in *Rock Fracture and Blasting, Theory and Applications*, Elsevier, Butterworth-Heinemann.

Zhu, Z., Mohanty, B. and Xie, H. (2007), "Numerical investigation of blasting-induced crack initiation and propagation in rocks", *Int. J. Rock Mech. Min. Sci.*, **44**(3), 412-424. https://doi.org/10.1016/j.ijrmms.2006.09.002.

JS